Available online at www.sciencedirect.com
ScienceDirect
Icarus 187 (2007) 296–305
ICARUS
www.elsevier.com/locate/icarus

Palomar and Table Mountain observations of 9P/Tempel 1 during the Deep Impact encounter: First results

James M. Bauer [a,*], Paul R. Weissman [a], Young-Jun Choi [a], Mitchell Troy [a], James W. Young [a], Carey M. Lisse [b], Richard Dekany [c], Martha S. Hanner [d], Bonnie J. Buratti [a]

[a] *Jet Propulsion Laboratory, California Institute of Technology, 4800 Oak Grove Drive, Mailstop 183-501, Pasadena, CA 91109, USA*
[b] *Johns Hopkins University, Applied Physics Laboratory, SD/SRE, MP3-W155, 7707 Montpelier Road, Laurel, MD 20723, USA*
[c] *Department of Astronomy, California Institute of Technology, 1200 E. California Blvd., Mail code 105-24, Pasadena, CA 91125, USA*
[d] *University of Massachusetts, Department of Astronomy, 619 Lederle Graduate Research Center, Amherst, MA 01003, USA*

Received 7 April 2006; revised 12 September 2006

Available online 16 January 2007

Abstract

We present the first results of the Palomar Adaptive Optics observations taken during the Deep Impact encounter with 9P/Tempel 1 in July 2005. We have combined the Palomar near-IR imaging data with our visual wavelength images obtained simultaneously at JPL's Table Mountain Observatory to cover the total wavelength range from 0.4 to 2.3 μm in the B, V, R, I, J, H, and K filter bands, spanning the dates from 2005 July 03–07. We also include in our overall analysis images taken on the pre-encounter dates of June 1 and June 15, 2005. The broad wavelength range of our observations, along with high temporal resolution, near-IR sensitivity, and spatial resolution of our imaging, have enabled us to place constraints on the temperature of the impact flash and incandescent plume of >700 K, and to provide mean dust velocities of order 197 ± 16 m/s approximately 1.25 h after impact derived from our 1.64 μm observations. Our ejected dust mass estimates, as derived from our near-IR observations, are an order of magnitude less than those previously reported for visual wavelength observations.

Keywords: Comet Tempel-1; Adaptive optics; Comets, dust

1. Introduction

Comets provide a critical part of our understanding of the formation and evolution of the Solar System. They serve as tracers of its primordial material (cf. Meech and Svøren, 2004) because they are comprised of the primitive materials from the locations where they formed in the early outer-planetary system. In the current broad understanding of cometary origins, many of these volatile-rich bodies were ejected from their formation regions. The accepted explanation is that a majority of these bodies originated at heliocentric distances of 5–35 AU, and were transported outward into the scattered disk and eventually the nether regions of the Solar System, the Oort cloud (cf. Dones et al., 2004) by perturbations with the giant planets. In contrast, the Kuiper Belt objects, beyond 35 AU, formed in situ (e.g., Levison and Morbidelli, 2003). Recent evidence suggests that the overall picture of comet evolution is not simple, though, in that the source regions of comets, such as the Kuiper Belt have evolved dynamically and physically (Morbidelli and Brown, 2004). Even the long period comets, with the majority of their lifetimes spent far from the Sun, undergo rapid collisional evolution (Dones et al., 2004) during the ejection process. Such evolution also includes depletion of volatiles and likely surface-mantling brought on by exposure to galactic cosmic rays, as well as brief periods of exposure to relatively more intense solar radiation during their perihelion approaches (Jewitt, 2002). Hence, all cometary surfaces undergo some degree of processing and evolution. As heliocentric distance is the dominant factor in terms of surface temperature, sublimation rates, and exposure to radiation from the solar wind, it is certain that the Jupiter-family comets (JFCs) like 9P/Tempel 1 have undergone a larger amount of processing owing to their comparative proximity to the Sun. However, the rates of the sur-

* Corresponding author.
E-mail address: bauer@scn.jpl.nasa.gov (J.M. Bauer).

0019-1035/$ – see front matter
doi:10.1016/j.icarus.2006.10.035

face evolution processes, like mantling, are also closely tied to the nature of the surface materials, the surface composition, and the surface and sub-surface volatile content (Jewitt, 2004). The density, size, compaction, and conductivity of any dust layer on the nucleus surface influence the rubble mantling rate. The surface composition and volatile content also influence the rate and effectiveness of irradiation mantling as well as the rate of surface darkening by interaction with the solar wind (Moroz et al., 2004). The rate of surface darkening may in turn affect the sublimation rate via the albedo's relation to surface temperature.

The Deep Impact mission was designed to provide planetary science with insights to core questions involving the study of cometary bodies, including their composition, origins, and evolution. The observations of the Deep Impact experiment were designed to yield constraints on the factors, such as the strength of the surface layers and their respective depths, that influence various evolutionary processes, such as mantling or collision-induced resurfacing. The experiment yielded these constraints by impacting the surface with a ∼370 kg mostly-copper projectile, with a velocity relative to the nucleus of 10.3 km/s, and excavating a quantity of material from the cometary nucleus interior (A'Hearn et al., 2005a). Spectra, taken prior to and during the impact event, contained compositional information for surface constituents and ejecta (A'Hearn et al., 2005a; Sunshine et al., 2006). The quantity of ejected dust provides direct constraints for the surface strength and the depth of the surface-layers deposited from historic activity. This quantity is best characterized and monitored from an Earth-based distance, and most practically from a number of ground-based observatories (Meech et al., 2005a), as the quantity of scattering dust per unit viewing solid angle is greater and therefore generates a more easily detectable signal. The field of view contains a much larger percentage of the dust emitted by the impact. The effects of solar radiation and the coma color distribution, which provide constraints on the nature of the dust, are apparent over the entire coma in observations taken at Earth–comet distances. Additionally, because spacecraft observations are limited in temporal range and resolution, viewing geometry, and often wavelength range, key observations come from the contribution of ground-based telescopes. Palomar Observatory was a major observing site in this ground-based network, and provided adaptive optics data in the J (with central wavelength, $\lambda_c = 1.25$ μm, and bandwidth $\delta_\lambda = 0.16$ μm), H ($\lambda_c = 1.64$ μm, $\delta_\lambda = 0.30$ μm), and K ($\lambda_c = 2.15$ μm, $\delta_\lambda = 0.31$ μm) filter bands, with its high spatial and temporal resolution over an essential wavelength range. These standard near-IR filter band passes were readily comparable with other cometary coma observations in the literature.

As part of the global effort by ground-based observatories to monitor the Deep Impact encounter with Comet 9P/Tempel 1, our observing team at Palomar and Table Mountain (TMO) Observatories covered the impact one night prior through three nights following the event. The Palomar 200-inch telescope played a crucial role in this campaign, in that it was the largest ground-based telescope to provide imaging in the near-infrared during the time of impact, offering temporal resolution on relatively short (approximately 11.4 s, including 9.9 s integration time and 1.5 s readout) time scales. Simultaneous visual-band observations were taken from TMO in the R-band during the impact event, and in the B, V, R, and I bands at times surrounding the event. We observed the comet with the Palomar 200-inch telescope using the PALAO system in adaptive optics mode at near-infrared wavelengths (Troy et al., 2000). Palomar's distinct AO system enabled us to obtain a near-IR data set with uniquely high spatial resolution, on average ∼0.8 arcsec seeing, FWHM, and at times down to 0.4 arcsec. The resolution afforded us the opportunity to better characterize other source contributions to the coma, differentiating between the ambient activity and that generated by the impact event. The AO data also allowed us to track changes in the coma and dust grains close-in to the nucleus during the impact, when ejecta were freshest. The changes that occurred in the dust coma on time scales of minutes to hours during the Deep Impact encounter can be best studied, at near-IR wavelengths, with an imaging data set such as this one. We present here preliminary results from our encounter observations during the night of the impact experiment, and briefly examine the ambient state of the comet from our monitoring campaign prior to the encounter as it pertains to these observations.

2. Observations and reduction

Table 1 lists a summary of our observations relating to the Deep Impact encounter. All nights reported here were photometric. Visual-band pre-impact observations were made on June 1 and June 15, 2005 at TMO prior to the DI encounter. During the encounter, TMO's 0.6-meter telescope also served as our visual-wavelength imaging site. Observations were made at TMO using a Bessel B, V, R, and I filter set in combination with the facility Photometric 1024×1024 CCD camera. The images have a plate-scale of 0.523 arcsec per pixel, and were flattened and bias-corrected in the usual manner (cf. Bauer et al., 2004) using the Image Reduction and Analysis Facility software package (IRAF; Tody, 1986). For each night's data, at least 9 bias frame zero-second exposures were averaged, with a 3-sigma pixel rejection algorithm. At least 5 sky-flat exposures per filter, taken at twilight, were median-combined to form a single flat for each band-pass. Bias frames were subtracted from each exposure, and each image was divided by the corresponding filter's flat frame. Calibrations were accomplished using Landolt equatorial standards (Landolt, 1992) to obtain zero-point, extinction, and color corrections. In order to guarantee coverage at the exact time-of-impact, we observed the comet through the R-band filter in drift-scan mode around the time of impact from 05:51:15 to 06:23:21 UT. We chose guiding rates of 15,000 arcsec per hour along each axis so that the comet drifted from the lower left (SE) corner of the CCD image to the upper right (NW) corner in two minutes, the length of our exposures. For all other times except the night of the impact, we tracked the comet at its predicted rate of motion across the sky, using values listed in an ephemeris obtained from JPL's Horizons service (http://ssd.jpl.nasa.gov). During the encounter run, we observed 9P/Tempel 1 to airmass values of ∼4 from TMO,

Table 1
9P/Tempel 1 observing runs at Palomar and Table Mountain Observatories

Dates (UT)	JD-2450000	Filter-bands	Seeing[a]	$PA_{\odot}$[b]	$PA_{vel.}$[b]	$\langle r \rangle$[c]	$\langle \Delta \rangle$[d]	Conditions
Jun 01	3522.6–3522.9	VRI	∼2.4 (TMO)	118	299	1.545	0.757	Photometric
Jun 15	3536.6–3536.9	K & VRI	1.0/1.8	114	302	1.519	0.807	Photometric
Jul 03	3554.6–3554.8	JHK & BVRI	0.48/2	112	304	1.506	0.889	Photometric
Jul 04	3555.6–3555.8	HK & BVRI	0.6/2	111	304	1.506	0.894	Photometric
Jul 05	3556.6–3556.8	HK & BVRI	0.7/2	111	305	1.506	0.899	Photometric
Jul 06	3557.6–3557.8	JHK & BVRI	0.7/2	111	305	1.506	0.904	Photometric
Jul 07	3558.6–3558.8	JHK & BVRI	0.6/2	111	305	1.506	0.910	Photometric

[a] *Approximate* FWHM in arcsecs for images (Palomar Obs./TMO, unless otherwise indicated).
[b] Position angles on the observer's sky plane of the Sun ⇒ comet radius vector ($PA_{\odot}$), and the negative of the comet's heliocentric velocity vector ($PA_{vel.}$) in degrees N through E as obtained from JPL's Horizons ephemeris service.
[c] Mean heliocentric distance (AU).
[d] Mean target–observer distance (AU).

and found a pre-impact R-band magnitude of ∼14.6, using a 5-arcsec aperture. The seeing degraded from our nominal value of 2 arcsec to ∼4 arcsec over this time. However, using relative photometry, we were able to correct for the seeing degradation to first order even when our object reached these low altitude angles.

We observed from Palomar using the near-IR PHARO camera in combination with the facility adaptive optics system (Hayward et al., 2001). The system utilizes a Shack–Hartmann high-order wave-front sensor (WFS) to guide and correct on bright objects, down to ∼13th (V-band) magnitude. The camera used a 1024 × 1024 Hawaii array, with a pixel scale of 0.04 arcsec for the configuration used. Pre-encounter estimates of 9P/Tempel 1's brightness were several magnitudes higher than the actual value during the 2005 perihelion approach, and so we were unable to effectively use the standard WFS, except when the comet appulsed a nearby bright star within ∼30 arcsec. The use of the WFS allows for correction of higher order optical distortion terms (cf. Hampton et al., 2003), and so is more desirable than the correction afforded by other wave-front sensors available at Palomar (see below). It should be noted, however, that the effectiveness of the WFS correction is dependent on the brightness of the WFS guide star, as well as the proximity of the guide star to the target, the intrinsic seeing, and the airmass of the target (Hayward et al., 2001). The correction may only be slightly better than for lower order terms alone, but we found that, during a bright guide star appulse, the correction was always better and more stable using the WFS. These appulse events occurred on the nights of July 3, 5, and 7 UT, but not on the night of the impact; it was during the appulse on July 3 that we achieved the best FWHM of 0.4 arcsec. We also obtained K-band exposures on June 15 at Palomar Observatory using the AO system's PHARO camera. We were unable to lock the AO correction loop on the faint comet, so the decision was made subsequent to the June 15 observations to hasten the implementation of a low-order wave-front sensor (LOWFS), that would allow guiding at fainter magnitudes, including those of the comet, while maintaining a lower degree atmospheric correction. As June 15 was an engineering night, no calibration star exposures were obtained, and so we only provide crude magnitude estimates for June 15 based upon the calibration data obtained during our Deep Impact encounter run.

For the encounter observations, the LOWFS worked on the first night it was tried, on July 3, achieving down to 0.5 arcsec resolution, and was used in all instances where a nearby bright star was not available for full AO correction, including the night of the Deep Impact encounter. Because the comet set below 4 airmasses at approximately 7 UT, we were allocated time for only the first half of the night, during which time we also had to obtain calibration star frames, twilight flats, and darks. Infrared standards were selected before the observing run from the literature (Persson et al., 1998; photometric standard Stars 9150, 9155, and 9178), and were observed at low and high airmass to correct for extinction, zero-point offset, and color terms. Because the coma was extended, sky frames 7 arcmin to the north of the comet's field of view (FOV) were taken within 20 min of any object exposure. This was seen as an adequate trade-off between tracking the changes in sky brightness and coverage of the event. Observations were restricted to H and K band filters during the night of the impact and the following night, July 5, as a balance between wavelength and temporal coverage. Individual frames were prepared using Palomar's AO IDL reduction software (AORED; https://s383.jpl.nasa.gov/~mtroy/AOred/), which rescales, median filters, and divides out flat frames, median filters and subtracts darks and sky frames, and rescales the object images to per-second signal values.

3. Analysis

3.1. Pre-impact observations

Prior to the encounter, TMO observations yielded magnitudes and $Af\rho$ values in V-, R-, and I-band filters for Comet 9P/Tempel 1 (Table 2). Measurements in an additional B-band filter were obtained in our July data. Our visual-band color data are rather typical of comets (cf. Tholen et al., 1981). The colors are similar to or slightly redder than solar colors, and do not vary much among the pre or post impact observations (Tables 3 and 4). Previous encounters averaged brightness values (total magnitude) near $m_R = 10$ when scaled to similar distances (Meech et al., 2005b; Belton et al., 2005) and $\log(Af\rho)$ [cm] values near 2.5 approximately 20 days prior to perihelion (Lisse et al., 2005), corresponding to our June 15 observations. Actual observations, however, yielded R-band $Af\rho$ values (A'Hearn

Table 2
9P/Tempel 1 visual pre-encounter magnitudes

Dates (UT)	m_V[a]	m_R	m_I	ρ [km]	$Af\rho$ [log cm]		
					V	R	I
June 01	15.395 ± 0.028	14.995 ± 0.048	14.589 ± 0.065	1.09×10^3	2.192 ± 0.011	2.208 ± 0.019	2.258 ± 0.026
	14.233 ± 0.006	13.775 ± 0.013	13.325 ± 0.023	2.76×10^3	2.254 ± 0.003	2.293 ± 0.005	2.361 ± 0.009
	13.467 ± 0.022	12.999 ± 0.002	12.521 ± 0.011	5.49×10^3	2.262 ± 0.009	2.305 ± 0.003	2.384 ± 0.004
	12.701 ± 0.006	12.303 ± 0.001	11.799 ± 0.001	1.10×10^4	2.267 ± 0.003	2.282 ± 0.003	2.371 ± 0.003
June 15	15.250 ± 0.010	14.765 ± 0.014	14.240 ± 0.015	1.16×10^3	2.263 ± 0.004	2.313 ± 0.006	2.411 ± 0.006
	14.090 ± 0.008	13.639 ± 0.014	13.140 ± 0.014	2.94×10^3	2.324 ± 0.004	2.361 ± 0.006	2.448 ± 0.006
	13.330 ± 0.008	12.904 ± 0.013	12.410 ± 0.014	5.84×10^3	2.330 ± 0.004	2.356 ± 0.005	2.442 ± 0.006
	12.590 ± 0.008	12.220 ± 0.013	11.710 ± 0.014	1.17×10^4	2.325 ± 0.004	2.329 ± 0.005	2.421 ± 0.006

[a] Corresponding to 2, 5, 10 and 20 arcsec radius apertures. Test data taken the night of June 15 at Palomar yielded a 2-arcsec aperture (radius) K-band mag. of 13.22 ± 0.11 and a 5-arcsec aperture mag. of 12.36 ± 0.11 corresponding to a $\log(Af\rho$ [cm]) value of 2.42 ± 0.04.

Table 3
Deep Impact event B–K colors (5 arcsec aperture)

Date (UT)	B–V[a]	V–R	V–I	m_V	J–H	H–K	H–K (2")	m_H	V–H
050703	0.83(±0.04)	0.34(±0.04)	0.87(±0.05)	14.58(±0.03)	0.43(±0.07)	0.32(±0.22)	0.31(±0.16)	12.51(±0.04)	2.07(±0.05)
050704									
Pre-impact	0.74(±0.03)	0.48(±0.03)	0.93(±0.03)	14.64(±0.03)	–	0.34(±0.04)	0.34(±0.05)	12.50(±0.06)	2.14(±0.07)
Impact + 7m					–	0.42(±0.11)	0.29(±0.05)	12.14(±0.05)	
Impact + 30m					–	0.31(±0.06)	0.21(±0.05)	11.56(±0.03)	
Impact + 65m					–	0.31(±0.05)	0.21(±0.05)	11.42(±0.03)	
Impact + 75m					–	0.29(±0.07)	0.21(±0.05)	11.45(±0.02)	
050705	0.84(±0.03)	0.36(±0.03)	0.90(±0.03)	14.25(±0.03)	–	0.53(±0.10)	0.29(±0.03)	12.33(±0.04)	1.92(±0.05)
050706	0.76(±0.03)	0.40(±0.03)	0.88(±0.03)	14.36(±0.03)	0.45(±0.07)	0.38(±0.15)	0.25(±0.10)	12.34(±0.04)	2.02(±0.05)
050707	0.79(±0.03)	0.43(±0.03)	0.90(±0.03)	14.48(±0.03)	–	0.42(±0.16)	0.29(±0.15)	12.46(±0.05)	2.02(±0.06)

[a] Approximate solar colors: B–V = 0.65, V–R = 0.36, V–I = 0.65 (Drilling and Landolt, 2000), J–H = 0.31, H–K = 0.06, V–H = 1.43 (Tokunaga, 2000).

Table 4
Deep Impact event V- and H-band magnitudes, $Af\rho$ values, and H–K colors

Date (UT)	m_V[a]	m_H[a]	$Af\rho_H$	$Af\rho_H$	V–H	H–K[b]	V–K
050615	14.09(±0.03)		2.32 ± 0.01				
050703	14.58(±0.03)	12.51(±0.04)	2.17 ± 0.01	2.42 ± 0.02	2.07(±0.05)	0.31(±0.16)	2.39(±0.17)
050704							
Pre-impact	14.64(±0.03)	12.50(±0.06)	2.15 ± 0.01	2.43 ± 0.02	2.14(±0.07)	0.34(±0.05)	2.48(±0.08)
Impact + 7m		12.14(±0.05)		2.57 ± 0.02		0.29(±0.05)	
Impact + 30m		11.56(±0.03)		2.80 ± 0.01		0.21(±0.05)	
Impact + 65m		11.42(±0.03)		2.86 ± 0.01		0.21(±0.05)	
Impact + 75m		11.45(±0.02)		2.85 ± 0.01		0.21(±0.05)	
050705	14.25(±0.03)	12.33(±0.04)	2.31 ± 0.01	2.50 ± 0.02	1.92(±0.05)	0.29(±0.03)	2.45(±0.11)
050706	14.36(±0.03)	12.34(±0.04)	2.26 ± 0.01	2.50 ± 0.02	2.02(±0.05)	0.25(±0.10)	2.40(±0.16)
050707	14.48(±0.03)	12.46(±0.05)	2.22 ± 0.01	2.45 ± 0.02	2.02(±0.06)	0.29(±0.15)	2.44(±0.17)

[a] 5-arcsec aperture radii.
[b] 2-arcsec aperture radii.

et al., 1984a) of 2.31 on June 1, and 2.35 on June 15, lower than were expected (Table 2). These values were derived from 5-arcsec aperture radius R-band magnitudes and include the signal of the nucleus. K-band magnitudes were obtained on the night of June 15th as well, yielding redder than solar V–K colors (V–K for the Sun is ∼1.49, while on June 15, the 9P/Tempel 1 V–K color was 1.73 ± 0.11). These redder colors at near-IR wavelengths were a persistent feature of the ambient comet, although the V–K colors were typically redder still (V–K ∼2.4; see Tables 3 and 4) during the encounter than on June 15. This may have been caused in part by large particles being injected into the coma by an outburst of 9P/Tempel 1, which was reported for the preceding night (A'Hearn et al., 2005a).

A three-color VRI-band composite image from June 1 is shown in Fig. 1. The coma is almost neutral (slightly red, according to the colors in Table 2) in color at visual wavelengths. Fig. 2 shows a color-composite at near-IR wavelengths taken on the night prior to impact, 21 h after the last reported outburst and before the impact experiment (A'Hearn et al., 2005a). J is mapped to blue, H to green, and K to red. The H-band AO-corrected seeing was only about ∼10% poorer than the K-band, comparing the FWHM values of on-frame bright stars,

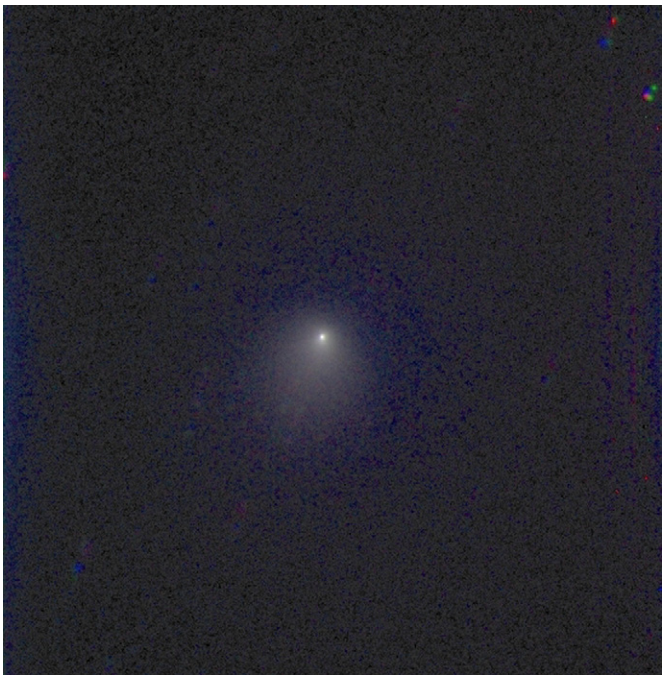

Fig. 1. Pre-encounter imaging of 9P/Tempel 1. The image, taken at TMO on June 1, 2005 (UT), shows the comet's neutral color and extended coma. The image is approximately 9 arcmin on a side, and (as with all the images shown) is displayed with E to the left and N up.

Fig. 2. Pre-encounter Palomar imaging of 9P/Tempel 1 taken ∼24 h prior to impact. The image is a composite of J (blue channel), H (green), and K band (red) exposures totaling 6 min each. The image has been color balanced so that solar colors should appear white. Also, the K-band image has been convolved with a Gaussian PSF to match the seeing FWHM in the H- and J-bands before combining the images to form the color composite. Hence, the comet's red appearance is indicative of a rather steep red spectral slope in its ambient state. The image is approximately 12 arcsec on a side, and (as with all the images shown) is displayed with E to the left and N up.

and the J-band had a seeing value ∼10% poorer than the H-band. Hence, the H- and K-band images have been convolved with Gaussian PSFs to match the seeing FWHM in the J-band before combining the images to form the color composite. The image suggests a near-IR color gradient, with the outer coma's brightness dropping off less steeply in the 1.25 and 1.64 μm band than in the K-band. Hence because phenomenon of the more extended coma at lower wavelengths is present at H as well as J, it is likely a true characteristic of the coma's color, and warrants future investigation.

3.2. Impact observations

The night of the impact we obtained simultaneous visual band and near-IR coverage from our two observatories, Palomar and TMO. Fig. 3 consists of two drift scan images of duration 120 s taken near the beginning of the impact experiment from TMO. The drift-scan method was used to obtain temporally-resolved coverage at the exact time of impact, such that the impact flash would be observed, or at least constrained, in the event that the flash or plume was not bright enough to detect. The left-hand image encompasses the time of impact, and the arrow indicates the time of impact to within about one second. No flash was obviously present in the drift scan image at the time of impact. Judging from the comet's brightening during the last quarter of its trail, our sensitivity was on the order of three tenths of the signal level, placing our upper limit for the flash brightness at >15.5 magnitudes, or $<1.1 \times 10^{-15}$ erg cm^{-2} s^{-1} Å^{-1} at 0.7 μm. Although a small amount of brightening is discernable at the position corresponding to 3 s prior to the impact time, we believe this falls outside the margin of error of our time estimate and attribute the brightening to noise. The right-hand panel shows continued brightening of the comet about 30 min after the impact. At that point the trail had brightened by a factor of ∼3 from pre-impact values. The relative brightening was derived from the count values in a 4-arcsec (8-pixel) box aperture, centered over the drift-scan trail's middle in the right panel's image, relative to a similar sampling of the pre-impact portion of the drift-scan trail from the left panel's image. Sky-count values were subtracted from each aperture signal before comparison. The steeper line in the second image is a satellite passing through the field of view.

The Palomar observations were tracked on the comet, taking individual exposures rather than drift-scans. Image exposure times were 9.9 s. The first image of the encounter impact, starting at 05:51:56 UT, bracketed the time of impact (05:52:02 UT), and ended 3–4 s after the impact. Fig. 4 shows difference images near the time of the encounter. The brightening was quickly obvious even at the telescope. The 10 images taken immediately prior to impact were averaged, co-aligned with respect to their brightness centroid sampled out to 0.4 arcsec, and subtracted from the series of 20 exposures, similarly co-aligned, taken following the impact (averaged together into 2 sets of 10). Time stamps for the central exposure are given in the figure caption. Extensions are to the northwest and to the southwest in the first panel (A), and the southwest extension is roughly consistent with the direction of the high velocity

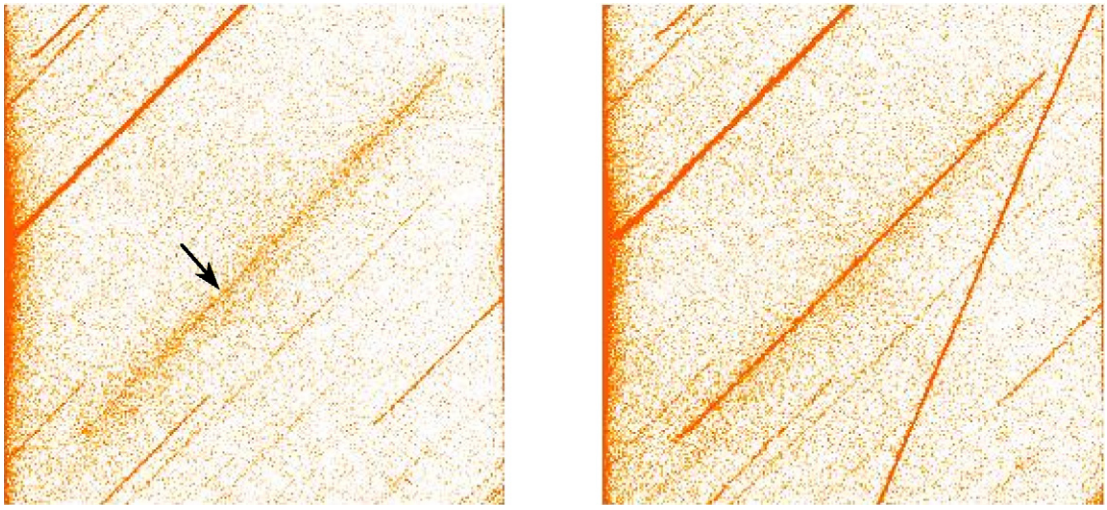

Fig. 3. Drift scan images of Comet 9P/Tempel 1 during the Deep Impact encounter. Left: 120 s R-band exposure begun at 05:51:15 on July 4 (UT). Comet drift is from lower left to upper right. The time of impact, 05:52:01.8 ± 0.4, is indicated by the arrow. No significant brightening of the trail is observed. Right: Similar drift scan image, 120 s in duration, begun at 06:21:21 UT, about 29 min after impact. The comet trail has brightened by about a factor of three. The steeper diagonal line at right is an Earth-orbiting satellite that passed through the field-of-view.

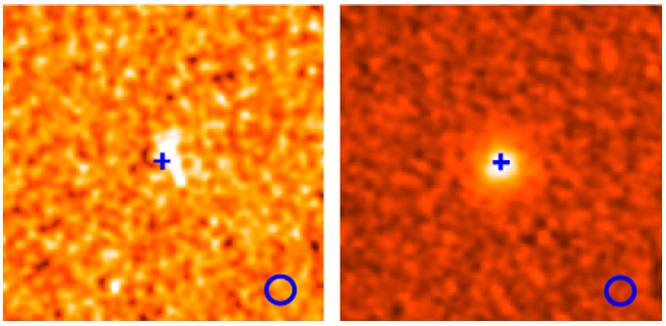

Fig. 4. The K-band image of the impact (right; 05:50:47–05:52:42 UT) and the image immediately following (left; 05:52:45–05:54:43 UT). Both images are the result of 10 co-added frames, with the co-added image taken immediately prior to the impact subtracted. The blue circle indicates the mean seeing disk size for the night's data, ∼0.7 arcsec in diameter, and the field of view of each image is 7 × 7 arcsec. The center of the brightness peak prior to subtraction is indicated by the blue cross-hairs.

ejecta, though it is unexpected that such features would be resolved so soon after the impact. Estimated ejection velocities of ∼10 km/s for the luminous plume would only extend to at most 400 km, neglecting projection effects, over the 40 s past impact that the first co-added image covers, while the southwest extension is >500 km. However, a similar extension to the south and west (position angle 225°, north through east, and also about an arcsec in length) was reported by other observers at mid-IR wavelengths (Meech et al., 2005a). Panel B shows the brightening within 2 min after impact (note the relative prominence of the constant background noise levels in the two panels). The brightening concentrated at the unresolved core has already swamped most lower-intensity features, though the brightening seems subtly to extend to the south and west.

The Palomar light curve for the night of the encounter is shown in Fig. 5. Panel A shows our data covering the night of the event and panel B shows the light curve a few minutes preceding and following the impact event. The magnitudes in panels A and B are plotted with respect to the integration mid-times, and K-band photometry for aperture radii of 0.5, 0.8, and 2.0 arcsec are shown along with H-band photometry for a 2-arcsec radius photometry aperture. The background was sampled at approximately 500–600 pixels (20–24 arcsec) from the comet. The first K-band data point following the dashed line indicating time-of-impact (corrected for light-travel time) actually contains the signal at the moment of impact near its center time. All apertures show two trends in the light curve within the first minute after the impact: an initial rapid increase, followed by a marked decrease in the rate of brightening approximately 50 s following the impact. A third trend seems possible at approximately 7 min in the form of a renewed increase in the brightening, but at a lower rate of increase than the initial rapid brightening. However, upon analysis of fitted line slopes to the 1 to 6 min and 7 to 20 min post-impact samples of the light curve points, the increase after 7 min is not significantly different than the rate observed after 50 s in the 0.5 and 2.0 arcsec apertures. The 0.8-arcsec aperture shows a difference in the rates before and after 7 min at the 2σ level. The times-of-change in the post-impact brightening rate are indicated by a vertical dot-dashed line in Fig. 5B. Signal from any impact flash is not readily apparent in the 2-arcsec aperture radius signal, and the 9.9-s integration following shows only a modest brightening in the largest of the apertures. The rate of brightening begins to decrease past 23 min, post-impact, and its decline is sharpest in the smallest aperture. The intervals of coverage of the TMO R-band visible data, shown in Fig. 4, are indicated for the corresponding exposure time spans by the cyan dashed lines in Fig. 5 (panels A and B).

Our preliminary color data from Palomar and TMO are given in Table 3. The near-IR colors show more variation than those of the visual bands. Photometry was obtained for the near-IR data using 2 and 5 arcsec aperture radii to compare with our visual data sets. The Palomar seeing varied between FWHM values of 0.5 and 1 arcsec. The TMO data set during the DI encounter

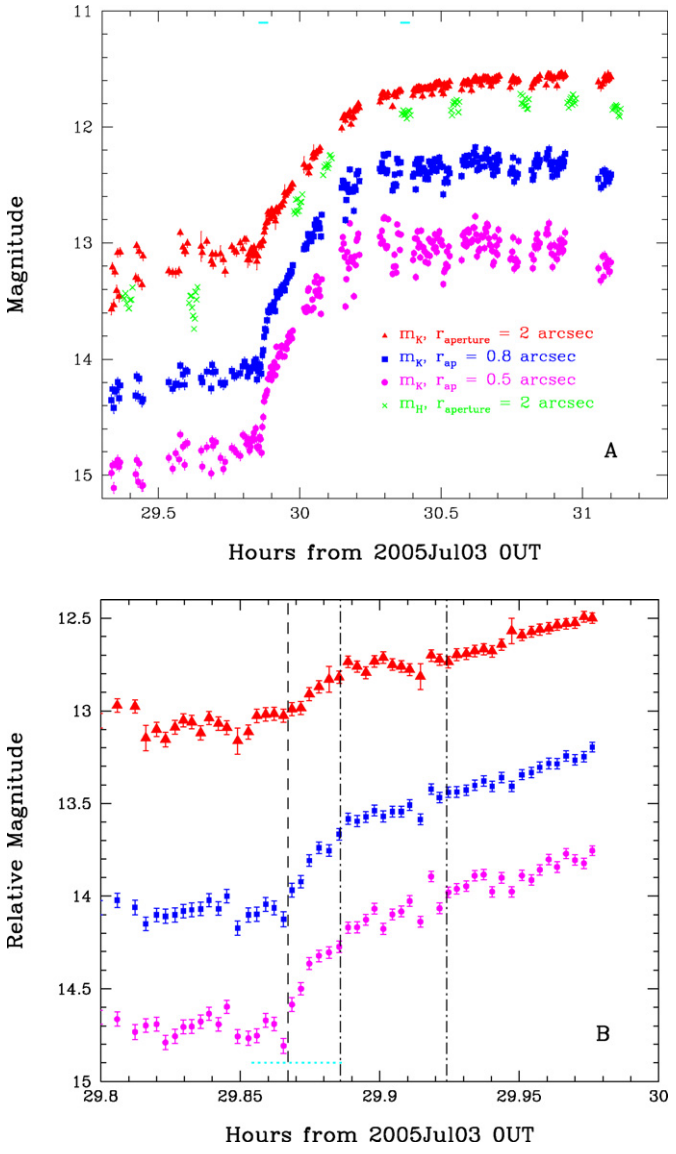

Fig. 5. The Palomar light curve of Comet 9P/Tempel 1 during the night of the Deep Impact experiment. The top panel (A) shows the entire data set for the impact night. The red points represent the 2.15 μm (K-band) magnitude of the comet within a 2 arcsec aperture radius from the brightness peak. 0.8 and 0.5 arcsec aperture signals for the K-band data are shown in blue and magenta, respectively. The 1.64 μm (H-band) data is shown in green. The K-band 2.0, 0.8, and 0.5 arcsec aperture signals are shown in detail at the time surrounding impact in the bottom panel (B). The time of impact is shown by the vertical dashed line. The approximate times of transition between the three stages of post-impact brightening, as indicated by the light curves, are shown by the dot-dashed lines. Note, however, the times of onset of the changes in the brightening rates may differ between individual aperture data sets, and while the rate of post-impact brightening may change at the farthest dot-dashed line on the right, the evidence of this is significant at the 2σ level only in the 0.8 arcsec aperture signal. The cyan dotted line at the bottom of the graph corresponds to the time interval of the first drift scan in Fig. 3.

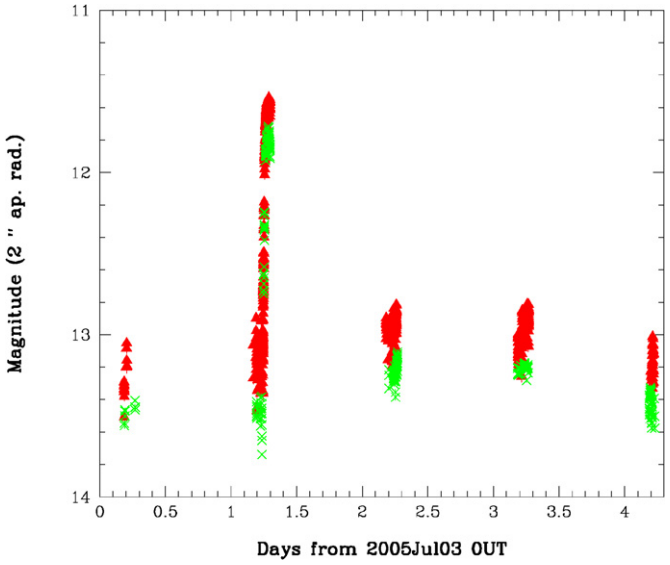

Fig. 6. The H- and K-band magnitudes over the five nights of coverage of the Palomar data set. By the night of July 7 (UT), the H- and K-band signals had returned to their pre-encounter levels.

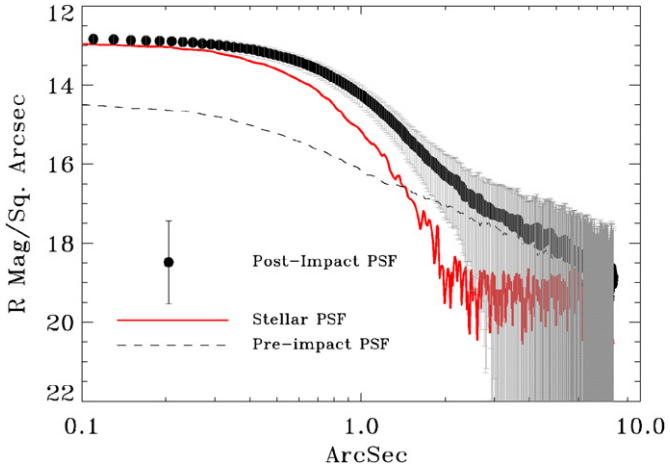

Fig. 7. The surface brightness profile of 9P/Tempel 1 immediately before and 67 min following impact at 1.65 μm. The values are plotted in units of H-band magnitudes on a log-angular-distance scale as black points with error bars. The red curve indicates the mean stellar profile provided by an average of background stars in the field at and near the time of the exposures, and re-scaled to the peak signal to show the extent of the coma. The lower dashed curve is the comet's profile taken approximately 15 min before the impact.

had seeing of between 2 and 4 arcsec, and so we compared only the 5-arcsec aperture values for our exposures taken during the encounter. Our H-band observations were taken within 6 min of our K observations. We took image following the sequence: 5 K-band observations, 10 H-band observations, 5 K-band observations. The 10 K-band observations, and the 10 H-band observations were then co-added, respectively, and H–K colors calculated. The changes in near-IR color roughly track those reported by Mori et al. (2006), although our average H–K colors appear somewhat larger by 0.05 to 0.1 magnitudes. In either case, the colors are slightly redder than may be expected from average active comet colors (cf. Veeder and Hanner, 1981; A'Hearn et al., 1981, 1984b; Campins et al., 1982; these yield a collected mean H–K color from 6 comets of $\sim 0.22 \pm 0.15$, and 0.41 ± 0.10 for the J–H mean), possibly owing to a thermal contribution from the grains at 2.15 μm (Hanner et al., 1984). The overall trends during the impact indicate bluer colors at near-IR wavelengths immediately following the impact, relative to pre-impact colors. This is true of the colors sampled in both the

smaller (2 arcsec radius) and larger (5 arcsec radius) apertures. However, the change in near-IR color is more pronounced in the smaller aperture values. In contrast, both apertures had comparable color values pre-impact.

3.3. Post-impact observations

The magnitudes of our data spanning July 03–07 are shown in Fig. 6. By the third night following the encounter, 9P/Tempel 1's brightness had dropped to levels at or below those taken one night prior to impact. Near-IR colors, listed in Table 3, show a most notable variation in the pre and post encounter colors for the night of the impact, which show a shift to the blue following the impact. As with all our colors, the background was sampled at approximately 500–600 pixels (20–24 arcsec) from the comet. At these distances, any signal in the near-IR was indistinguishable from the background (see Fig. 7). The data on July 5 indicated colors in the 2-arcsec radius aperture approaching the pre-encounter colors, but in the 5-arcsec radius aperture, colors were actually redder than the pre-encounter levels. A search for background stars in the signal or sky sampling has been negative. By our last night of observations, the July H–K colors and magnitudes in all aperture sizes were approaching their pre-impact values.

4. Discussion

Many of the unique details that this data set offers are shown in the light curves. Three stages of the impact brightening have been reported by Meech et al. (2005a), who place all three stages within a window of 7 min. However, the timing of the stages seem to vary, possibly according to the wavelength of the observations. The three possible stages in our data set also transpire within the first seven minutes after the impact. The intensity and the slope of the stages also vary with the aperture size in our own data set, possibly owing to propagation of the dust or plume material outwards, as well as sensitivity to the change based on aperture size. It is worth noting that none of the aperture diameters we use were smaller than 1.5 times the median seeing (0.65 arcsec, FWHM) with the Palomar AO system's LOWFS for the night of the impact, so that most (>85%) of the light generated by impact-related phenomena fell within our apertures. Our smallest aperture, with a 0.5 arcsec radius, has a projected distance of 320 km at the comet, a radius traveled in ∼40 s by the incandescent plume gases (A'Hearn et al., 2005a). It took the dust 30–60 min to travel this same distance according to estimates of dust velocities already in the literature (e.g., Küppers et al., 2005; Schleicher et al., 2006).

The initial brightening in our light curve associated with the first 3–4 s of the impact warranted further investigation. The Wien's peak wavelength for a blackbody at 1350 K is at the center of our K-band wavelength. If there were a flash that was observable from the ground, with a temperature range between 1000 and 2000 K (A'Hearn et al., 2005a), Palomar's AO system would be optimal for observing it. We measured the photometry in apertures with radii of 0.5, 0.6, 0.7, and 0.8 arcsec, and interpolated between the last pre impact and the second and third post impact points. The values for the first exposure, covering the impact event, yielded an excess from the line fits of $\sim 0.061 \pm 0.013$ magnitudes, which converts to $\sim 8(\pm 1.7) \times 10^{-9}$ erg cm^{-2} s^{-1} sr^{-1} Å^{-1}, if we take the upper limit of the size of the incandescent plume as 300 m (A'Hearn et al., 2005a). This would yield a lower limit of temperature between 700 and 900 K. This lower bound is in line with the mid-IR spectroscopic observations reported by A'Hearn et al. (2005a) that yielded impact flash temperatures of ∼1000–2000 K. Furthermore, radiative energy from a 900 K plume of duration ∼0.2 s, as implied by the duration of the spectroscopic plume signal from the Deep Impact spacecraft's High Resolution Instrument (A'Hearn et al., 2005a), would mean that approximately 1% of the total of approximately 2500 GJ of impact energy (A'Hearn et al., 2005b) was emitted radiatively. That fraction of the impact energy partitioned into radiation, rather than mechanical energy, is nearly an order of magnitude greater than what was predicted as the maximum of the widely unconstrained values in the literature (Buratti and Johnson, 2003), and consistent with the fact that Deep Impact's camera was saturated by the flash.

The surface brightness profile (SBP) of a series of 10 co-added H-band images, taken 67 min after the impact is shown in Fig. 7. For comparison, a stellar profile is shown in red, rescaled to the comet's peak value, and the comet's surface brightness profile prior to the impact is shown in gray. Near a distance of 1.2 arcsec, the SBP shows a change in slope, steepening closer inward. This distance is over twice the half-width of the stellar PSF for the image, and is likely caused by the expansion of the dust ejecta impact plume out to these distances, placing an approximate velocity for the dust at 197 ± 60 m/s.

Another means of deriving this value is by further image analysis. Taking our last co-added H-band image for the night, we divided out the azimuthal average about the brightness peak (see Schleicher and Farnham, 2004). The remaining features of the dust coma seen in Fig. 8 appear to be the impact ejecta front moving outwards from the nucleus, especially when compared to similarly processed images taken sooner after impact. The crosses demarcate the 3σ signal level relative to the image background. Using this as an upper-bound on the progress of the dust propagation gives a velocity for the dust of 212 m/s. The peak feature, located closer to the center, yields an average velocity of the associated dust of 181 m/s over the first 75 min. The mean of these two velocities is 197 ± 16 m/s, neglecting projection effects.

Estimates of the dust production can also be derived from our observations. Our near-IR data set is of particular value in that it is more sensitive to larger grain sizes (in excess of ∼0.7 μm; cf. Bohren and Huffman, 1998). We may use $Af\rho$ as a proxy for the quantity of dust ejected (A'Hearn et al., 1984a), or we may derive the mass of the dust (M_{dust}) from the $Af\rho$ value using the relation:

$$M_{\text{dust}} = \Sigma\left(4/3\pi a^3\sigma\right)/\left(\pi a^2\right) \tag{1}$$

and

$$\Sigma \approx Af\rho(\pi\rho/4p) \tag{2}$$

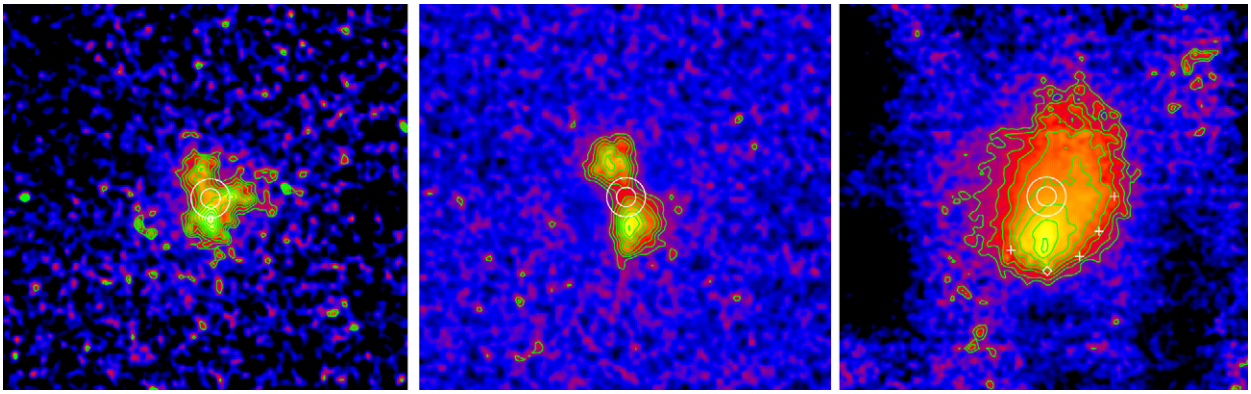

Fig. 8. H-band images from the night of the impact, taken 7, 30, and 75 min (left to right) following the impact. The images have been processed by dividing out the azimuthal-average of each frame about the brightness peak, the location of which is indicated by the two white concentric circles, which also indicate the size of 0.5 and 0.8-arcsec resolution elements. The images are approximately 10 arcsec on a side, and reveal the outward propagation of impact-related brightness extensions, and the propagation of the dust brightness peak. The white crosses and diamond represent the 3σ signal level above the background along the dust propagation front.

(Fulle, 2004), where Σ is the total dust cross section in the aperture ρ, a is the mean particle size, σ the mean grain density, and p is the effective grain reflectance (Meech and Weaver, 1996; Bauer et al., 2003). However, the model assumes no significant contribution from the nucleus or ambient coma to the $Af\rho$ values derived from the magnitudes. The first assumption may be used as an adequate first-order approximation provided our aperture is smaller than the dust propagation distance. We can correct for this using the propagation distance as the effective aperture in our $Af\rho$ calculations, and again assuming that the signal we use is from the ejected dust alone. Therefore, in order to estimate the mass of dust liberated by the impact, it is necessary to subtract out the contribution from the ambient coma and the nucleus, which we may do using our July 4 pre-impact values. This, in combination with the modified aperture size, 1.5 arcsec, using the values for the series of images taken 75 min after impact (Table 4), yields a modified $Af\rho$ value, for grain sizes on the same order as the observing wavelength, of 2100 cm, and a total mass on the order of 2×10^5 kg. This assumes a dust grain radius of $\sim$0.7 μm, a grain density of $\sim$1 g cm^{-3}, and a grain albedo of $\sim$0.1. This is an order of magnitude less than that reported using visual band data (Meech et al., 2005a), and may be indicative of a dust grain size distribution weighted toward smaller sizes, at least in the contribution to the coma from the impact. This is also consistent with the "bluer" colors observed in the near-IR during the impact.

5. Conclusions

- Observations prior to impact indicated that the comet was less active near perihelion than previously observed, including dust production below what was predicted for 9P/Tempel 1's 2005 perihelion approach, based on previous apparitions.
- Color photometry from 0.5 to 2.0 μm shows evidence of slightly redder-than-solar colors, and a shift of the comet colors blueward was apparent in the near-IR soon after impact. By July 7 (UT), the NIR colors had returned to pre-encounter values within our measurement error.
- No moment-of-impact flash was apparent in the TMO visual-band data set. However, the Palomar near-IR data set show some interesting signs of initial brightening, discontinuous with other trends. This brightening would be consistent with a flash or incandescent plume at impact with temperatures in excess of 700–900 K.
- Brightening rate changes are evident in the light curve within seven minutes after the encounter event. The steepest rate occurs initially, and smaller apertures show a faster rate of increase. A second, subtle increase in the post-impact brightening rate may occur after 7 min, although our strongest evidence for a slope change is at the 2σ level. The interval of 7 min for all 3 stages is roughly consistent with that previously reported, as by Meech et al. (2005a).
- Coma morphology changes attributable to the impact are evident close in to the comet's nucleus. Post-impact coma extensions have been measured to yield a mean dust ejection velocity, as projected on to the plane of the sky, of $\sim 197 \pm 16$ m/s.
- Estimates of the ejected dust mass made from our data set are $\sim 10^5$ kg, an order of magnitude less than previously reported estimates. These estimates, applicable to grain-sizes with radii $\sim$0.7 μm, are smaller than those reported in the visual, and so may suggest the impact generated dust was dominated by small grains, although bimodal or other dust-grain size distributions may also be responsible.

Acknowledgments

We thank the superlative efforts of Palomar Observatory and its staff, and the Palomar AO team, for providing observing time and support for these observations. We are also grateful for the helpful suggestions of our reviewers S. Lederer and T. Farnham. Table Mountain Observatory is operated under internal funds provided by JPL's Science and Technology Management Council. This work was performed in part at the Jet Propulsion Laboratory under contract with NASA. It was funded in part by the NASA Planetary Astronomy Program.

References

A'Hearn, M.F., Schleicher, D.G., Millis, R.L., Feldman, P.D., Thompson, D.T., 1984a. Comet Bowell 1980b. Astron. J. 89, 579–591.

A'Hearn, M.F., Dwek, E., Tokunaga, A.T., 1984b. Infrared photometry of Comet Bowell and other comets. Astrophys. J. 282, 803–806.

A'Hearn, M.F., Dwek, E., Tokunaga, A.T., 1981. Where is the ice in comets. Astrophys. J. 248, L147–L151.

A'Hearn, M.F., and 32 colleagues, 2005a. Deep Impact: Excavating Comet Tempel 1. Science 310, 258–264.

A'Hearn, M.F., Belton, M.J.S., Delamere, A., Blume, W.H., 2005b. Deep Impact: A large-scale active experiment on a cometary nucleus. Space Sci. Rev. 117, 1–3.

Bauer, J.M., Fernández, Y.R., Meech, K.J., 2003. An optical survey of the active Centaur C/NEAT (2001 T4). Publ. Astron. Soc. Pacific 115, 981–989.

Bauer, J.M., Buratti, B.J., Simonelli, D.P., Owen, W.M., 2004. Recovering the rotational light curve of Phoebe. Astrophys. J. 610, L57–L60.

Belton, M.J.S., and 15 colleagues, 2005. Deep Impact: Working properties for the target nucleus Comet 9P/Tempel 1. Space Sci. Rev. 117, 137–160.

Bohren, C.F., Huffman, D.R., 1998. Absorption and Scattering of Light by Small Particles. Wiley, New York.

Buratti, B.J., Johnson, L.L., 2003. Identification of the lunar flash of 1953 with a fresh crater on the Moon's surface. Icarus 161, 192–197.

Campins, H., Rieke, G.H., Lebofsky, M.J., 1982. Infrared photometry of periodic Comets Encke, Chernykh, Kearns–Kwee, Stephan–Oterma, and Tuttle. Icarus 51, 461–465.

Drilling, J.S., Landolt, A.U., 2000. Normal stars. In: Cox, A.N. (Ed.), Allen's Astrophysical Quantities. Springer-Verlag, New York, pp. 339–375.

Dones, L., Weissman, P.R., Levison, H.F., Duncan, M.J., 2004. Oort cloud formation and dynamics. In: Festou, M.C., Keller, H.U., Weaver, H. (Eds.), Comets II. Univ. of Arizona Press, Tucson, pp. 153–174.

Fulle, M., 2004. Motion of cometary dust. In: Festou, M.C., Keller, H.U., Weaver, H. (Eds.), Comets II. Univ. of Arizona Press, Tucson, pp. 565–575.

Hayward, T.L., Brandl, B., Pirger, B., Blacken, C., Gull, G.E., Schoenwald, J., Houck, J.R., 2001. PHARO: A near-infrared camera for the Palomar Adaptive Optics system. Publ. Astron. Soc. Pacific 113, 105–118.

Hampton, P., Veran, J., Bradley, C., Hilton, A., Agathoklis, P., 2003. Adaptive optics control system development. In: Tyson, R.K., Lloyd-Hart, M. (Eds.), Astronomical Adaptive Optics Systems and Applications. In: Proc. SPIE, vol. 5169. SPIE, Bellingham, WA, pp. 321–330.

Hanner, M.S., Tokunaga, A.T., Veeder, G.J., Ahearn, M.F., 1984. Infrared photometry of the dust in comets. Astron. J. 89, 162–169.

Jewitt, D.C., 2002. From Kuiper Belt object to cometary nucleus: The missing ultrared matter. Astron. J. 123, 1039–1049.

Jewitt, D.C., 2004. From cradle to grave: The rise and demise of the comets. In: Festou, M.C., Keller, H.U., Weaver, H. (Eds.), Comets II. Univ. of Arizona Press, Tucson, pp. 659–676.

Küppers, M., and 40 colleagues, 2005. A large dust/ice ratio in the nucleus of Comet 9P/Tempel 1. Nature 437, 987–990.

Landolt, A.U., 1992. UBVRI photometric standard stars in the magnitude range 11.5–16.0 around the celestial equator. Astron. J. 104, 340–371.

Levison, H.F., Morbidelli, A., 2003. The formation of the Kuiper Belt by the outward transport of bodies during Neptune's migration. Nature 426, 419–421.

Lisse, C.M., and 17 colleagues, 2005. Spitzer and Chandra observations of the Deep Impact encounter with Comet 9P/Tempel 1. Bull. Am. Astron. Soc. 37. 1484.

Meech, K.J., Svøren, J., 2004. Using cometary activity to trace the physical and chemical evolution of cometary nuclei. In: Festou, M.C., Keller, H.U., Weaver, H. (Eds.), Comets II. Univ. of Arizona Press, Tucson, pp. 317–335.

Meech, K.J., Weaver, H.A., 1996. Unusual comets (?) as observed from the Hubble Space Telescope. Earth Moon Planets 72, 119–132.

Meech, K.J., and 208 colleagues, 2005a. Deep Impact: Observations from a worldwide Earth-based campaign. Science 310, 265–269.

Meech, K.J., A'Hearn, M.F., Fernández, Y.R., Lisse, C.M., Weaver, H.A., Biver, N., Woodney, L.M., 2005b. The Deep Impact Earth-based campaign. Space Sci. Rev. 117, 297–334.

Morbidelli, A., Brown, M.E., 2004. The Kuiper Belt and primordial evolution of the Solar System. In: Festou, M.C., Keller, H.U., Weaver, H. (Eds.), Comets II. Univ. of Arizona Press, Tucson, pp. 175–192.

Mori, Y., Sekiguchi, T., Sugita, S., Matsunaga, N., Fukushi, H., Kaneyasu, N., Kawadu, T., Kandori, R., Nakajima, Y., Tamura, M., 2006. Near-IR monitoring observation of Comet 9P/Tempel 1. Lunar Planet. Sci. 37. Abstract 2458.

Moroz, L., Baratta, G., Strazzulla, G., Starukhina, L., Dotto, E., Barucci, M.A., Arnold, G., Distefano, E., 2004. Optical alteration of complex organics induced by ion irradiation. 1. Laboratory experiments suggest unusual space weathering trend. Icarus 170, 214–228.

Persson, S.E., Murohy, D.C., Krzeminsky, W., Roth, M., Rieke, M.J., 1998. A new system of faint near-infrared standard stars. Astron. J. 116, 2475–2488.

Schleicher, D.G., Farnham, T., 2004. Photometry and imaging of the coma with narrowband filters. In: Festou, M.C., Keller, H.U., Weaver, H. (Eds.), Comets II. Univ. of Arizona Press, Tucson, pp. 449–469.

Schleicher, D.G., Barnes, K.L., Baugh, N.F., 2006. Photometry and imaging results for Comet 9P/Tempel 1 and Deep Impact: Gas production rates, postimpact light curves, and ejecta plume morphology. Astron. J. 131, 1130–1137.

Sunshine, J.M., and 22 colleagues, 2006. Exposed water ice deposits on the surface of Comet 9P/Tempel 1. Science 311, 1453–1455.

Tholen, D.J., Tedesco, E.F., Larson, S.M., 1981. Broad-band spectrophotometry of cemetary comae. Bull. Am. Astron. Soc. 13, 707.

Tokunaga, A.T., 2000. Infrared astronomy. In: Cox, A.N. (Ed.), Allen's Astrophysical Quantities. Springer-Verlag, New York, pp. 143–164.

Tody, D., 1986. The IRAF data reduction and analysis system. In: Instrumentation in Astronomy VI. Part 2. In: Proc. SPIE. SPIE, Bellingham, WA, p. 733.

Troy, M., Dekany, R.G., Brack, G., Oppenheimer, B.R., Bloemhof, E.E., Trinh, T., Dekens, F.G., Shi, F., Hayward, T.L., Brandl, B., 2000. Palomar adaptive optics project: Status and performance. In: Wizinowich, P.L. (Ed.), Adaptive Optical Systems Technology. In: Proc. SPIE, vol. 4007. SPIE, Bellingham, WA, pp. 31–40.

Veeder, G.J., Hanner, M.S., 1981. Infrared photometry of Comets Bowell and P/Stephan–Oterma. Icarus 47, 381–387.